Up-converted photoluminescence from CH$_3$NH$_3$PbI$_3$ perovskite semiconductors: Implications for laser cooling

Takumi Yamada, Tomoko Aharen, and Yoshihiko Kanemitsu[*]

Institute for Chemical Research, Kyoto University, Uji, Kyoto 611-0011, Japan

Up-converted photoluminescence (PL), or, in other words, anti-Stokes PL via phonon absorption in semiconductors is a critical property for realizing optical refrigeration. Here, we investigate the anti-Stokes PL from optically thin films and thick crystals of CH$_3$NH$_3$PbI$_3$ to assess their potential for laser cooling. Using PL excitation spectroscopy, we determine the excitation photon energy that maximizes the cooling efficiency. The evaluated up-conversion gain for the thick single crystal is close to 70% of that for the thin film, indicating a possibility for laser cooling even in thick crystals. We discuss the competition between anti-Stokes PL and photon reabsorption in CH$_3$NH$_3$PbI$_3$.

I. INTRODUCTION

In recent years, the lead halide perovskite semiconductors have been receiving significant attention as a novel material for optical devices. For example, the conversion efficiencies of the CH$_3$NH$_3$PbI$_3$ (methylammonium lead iodide, MAPbI$_3$)-based solar cells improved with a surprisingly fast pace when compared with other solar cell materials, and now have reached already as high as 23.7% [1–4]. These high conversion efficiencies of the perovskite solar cells are considered as a result of the perovskites's excellent optical properties (for example, the strong direct band transitions with a sharp absorption edge resulting from low defect densities, and the long carrier lifetime and diffusion length) [5–10]. Especially due to the highly efficient photoluminescence (PL) with almost no energy shift between the PL peak and the absorption edge, the phenomenon of repeated photon emission and reabsorption, i.e., photon recycling, occurs. The photon recycling in the perovskites has been initially observed in MAPbI$_3$ single crystals [11], and the utilization of the photon recycling effect in improving device efficiencies has been intensively discussed [12–20]. In the course of these discussions, it has been pointed out that the perovskite semiconductors have an internal luminescence efficiency of almost 100% [13].

One of the optical phenomena in semiconductors induced by extremely high luminescence efficiencies is laser cooling. The laser cooling induced by up-converted PL enables novel applications such as optical refrigerators, which have already been investigated for a relatively long time [21]. Laser cooling of solids has initially been realized with rare-earth-doped materials [22–24]. In the meantime, theoretical considerations also suggested a possible cooling of semiconductors due to band-to-band transitions [25]. However, a net cooling of semiconductors has hardly been observed in the experiments [26–28]. One important factor for achieving laser cooling is a high external quantum efficiency (EQE), but this is not the only factor because net cooling has not been achieved even for a GaAs/GaInP quantum-well sample with an EQE of 99.5% [28]. On the other hand, net cooling has recently been demonstrated for lead halide perovskites [29]. This is actually surprising, because these two materials, GaAs and lead halide perovskites, have very similar PL and absorption properties [8,30]. It is an open question why laser cooling is difficult to achieve in the III–V semiconductors [26–28] but perovskites can be cooled down very effectively [29]. Therefore, it is important to clarify the material properties and experimental conditions required for laser cooling. After elucidation of these factors, the physics of the laser cooling process can be clarified. The concept of laser cooling in semiconductors is based on up-converted PL [25]. Therefore, evaluation of the up-converted PL properties is necessary to study the cooling mechanism.

Usually, most of the up-converted PL cannot be extracted from optically thick samples due to a strong reabsorption which leads to sample heating. For this reason, the previous investigations on laser cooling in bulk semiconductors were performed on thin samples [26–29]. However, if the internal quantum efficiency is close to 100%, the external luminescence efficiency due to photon recycling also approaches 100% [31]. Consequently, it is expected that laser cooling occurs even in thick samples of highly luminescent materials such as the perovskite semiconductors. Also for designing optical refrigerators, it is important to clarify the physics of anti-Stokes PL (AS-PL) and its reabsorption in the perovskite by employing both optically thin and thick samples. However, the accurate evaluation of the AS-PL and laser cooling properties of optically thick samples requires a new experimental approach.

In this work, we prepared an optically thin film and thick single crystal of MAPbI$_3$, and compared their AS-PL

*kanemitu@scl.kyoto-u.ac.jp

characteristics. The AS-PL was clearly observed for both samples, and we divided the PL spectrum into anti-Stokes and Stokes parts. We characterized the excitation-energy dependence of the AS-PL and the Stokes PL (S-PL) using PL excitation (PLE) spectroscopy. For the analysis, we define E_{eq} as the excitation photon energy where the anti-Stokes PLE (AS-PLE) and Stokes PLE (S-PLE) intensities become equal. We introduce an up-conversion gain spectrum defined by the intensity difference between the AS-PLE and S-PLE spectra. The obtained spectrum is broad and its maximum lies at a point where E_{ex} is 11 meV below the E_{eq} of either sample. Theoretically, it can be considered that the cooling efficiency is highest at this point. The broad shape of the up-conversion gain spectrum implies that large anharmonic and overdamped phonon play an important role for the efficient up-conversion process in the perovskites.

II. EXPERIMENTAL

A. Samples

The thin-film sample was fabricated with the spin-coating method based on Ref. [32]. The thick single-crystal sample was obtained using the inverse temperature crystallization method based on Ref. [33]. During the measurements, the samples were mounted in an acryl box filled with nitrogen, and thus exposure to atmosphere was avoided. Additionally, in case of the single crystal, we prepared a clean surface by cleaving the sample prior the measurement. The thickness of the thin film was 400 nm and that of the single-crystal samples was 1.5 mm.

B. Photoluminescence excitation spectroscopy

The PLE spectrum measurements were performed at room temperature. For the light source, we used a supercontinuum white-light source with a repetition rate of 40 MHz. The white light passed through a monochromator and then was used as excitation light. The excitation light beam and the detected light were coaxially aligned with a broadband polarizing beam splitter cube. To focus the light on the sample, we used a near-infrared objective lens with a magnification of factor 5 and a numerical aperture of 0.14. We monitored the excitation light intensity for each wavelength through inserting a power meter after the objective lens, and by controlling a motorized circular variable neutral density filter the excitation power was adjusted to a single value for all wavelengths. The detected light was introduced into a spectrometer by using a fused silica lens with $f = 200$ mm. The PL spectra were measured with a nitrogen-cooled charge-coupled device array. The excitation light that entered the spectrometer was cut with a polarizer.

III. RESULTS AND DISCUSSION

A. Excitation-energy dependence of PL spectra

In Figures 1(a) and 1(b) we show the two-dimensional PLE maps of the MAPbI$_3$ thin film and the thick single-crystal sample, respectively. The vertical axis corresponds to the excitation energy, and the horizontal axis to the emission energy. The line in the diagonal direction is the scattered

excitation light. We note that the PL intensity is scaled by the excitation photon flux. As can be clearly seen in the figure, a different behavior was observed between the thin film and the single crystal. With the following detailed analysis of the PLE maps, we discuss the effect of photon reabsorption as well as the AS-PL.

In Fig. 1(c) we show five representative PL spectra of the MAPbI$_3$ thin film. The corresponding excitation energies employed here were 1.72, 1.64, 1.60, 1.58, and 1.57 eV. As can be clearly confirmed from the figure, the spectral shape of the PL is independent of the excitation energy and remains unchanged. A dominant luminescence from sub-band-gap states (defects or traps) would imply that these PL spectra redshift as the excitation energy decreases, which is not observed. Therefore, the PL spectra with a full width at half maximum of about 90 meV are a result of intrinsic broadening induced by electron-phonon coupling [20,34]. Especially in the case of excitation energies below 1.6 eV, a clear emission of AS-PL was observed.

The same analysis was also performed for the single crystal. In Fig. 1(d) we show five representative PL spectra of the thick MAPbI$_3$ single crystal. The corresponding excitation energies employed here were 1.65, 1.57, 1.53, 1.51, and 1.50 eV. The PL spectra observed from the single crystal were overall redshifted with respect to the thin film. This can be explained with the carrier diffusion effect, which appears as a result of the long carrier lifetime, and the reabsorption effect [11] (a detailed discussion is provided in Appendix A). The excitation energy and the PL peak energy coincide near 1.53 eV, and under excitation with energies below this value, AS-PL was also observed even in the single crystal.

In Fig. 1(e) we show the PL peak positions obtained for each of the used excitation wavelengths. When we focus on the data of the thin film, we find that the PL peak does not depend on the excitation energy, i.e., it is constant. More importantly, even when the excitation energy becomes smaller than the PL peak energy (1.6 eV), a constant value is maintained. When we consider that the reported band-gap energy of MAPbI$_3$ is 1.61 eV [7,35,36], this constant peak energy indicates that the excitation photons with energy below the band gap are absorbed by the assistance of phonons, and a dominant band-edge luminescence is observed.

Next, we focus on the data obtained from the thick single crystal. In the range above about 1.6 eV, the PL peak is near 1.552 eV and maintains an almost constant value. This range corresponds to excitation energies above the band gap, and therefore the penetration depth for the excitation light is small. The long diffusion length in MAPbI$_3$ single crystals [10] implies that the carrier diffusion length determines the distribution of the excited carriers and the PL peak energy becomes almost constant. When the excitation energy becomes smaller than ≈1.6 eV, the PL peak redshifts accordingly. Especially below the vicinity of 1.57 eV, it changes almost linearly with respect to the excitation energy. In this range, the absorption is determined by the so-called Urbach tail, an exponentially decaying value of the absorption coefficient for excitation energies below the band gap [8,37]. Here, the light penetration depth increases significantly and can exceed the diffusion length. Therefore, we can expect that the PL peak position reflects the penetration depth of the excitation light [19]. When
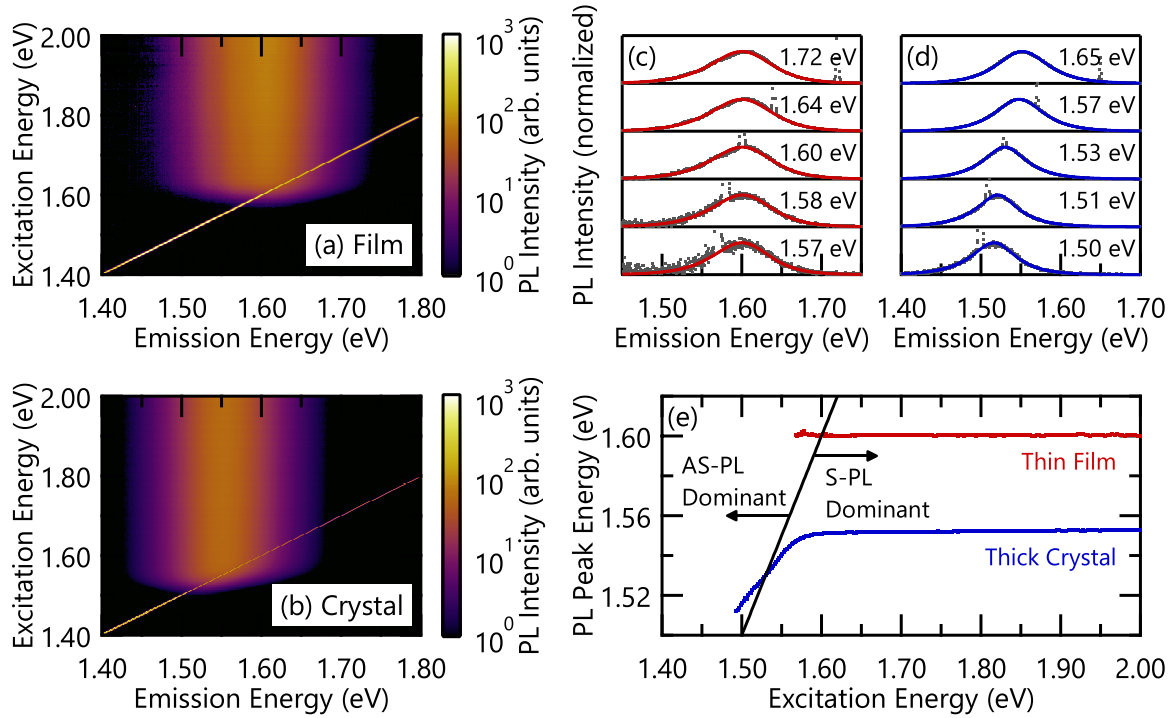
FIG. 1. (a) Two-dimensional PLE map of the MAPbI$_3$ thin film. (b) Two-dimensional PLE map of the MAPbI$_3$ thick single crystal. (c) Five representative PL spectra of the MAPbI$_3$ thin film. The corresponding excitation energies employed here were 1.72, 1.64, 1.60, 1.58, and 1.57 eV. (d) Five representative PL spectra of the MAPbI$_3$ thick single crystal. The corresponding excitation energies employed here were 1.65, 1.57, 1.53, 1.51, and 1.50 eV. (e) Excitation-energy dependences of the PL peak energies. The red and blue dot lines show the dependences for the thin film and thick single crystal, respectively. The black line corresponds to the excitation energy. The right side of this line corresponds to S-PL dominant region, and the left side corresponds to AS-PL dominant region.

we consider the physics of the thin film, the up-converted PL should become dominant for excitation energies below 1.6 eV. However, through the influence of photon reabsorption in the single-crystal sample, still a dominant S-PL is observed in the range of excitation energies above 1.53 eV. This tendency is readily obtained by the reabsorption model as explained in Appendix E. In the range of excitation energies below 1.53 eV, the PL changes to a dominant AS-PL.

B. Stokes and anti-Stokes PL properties

With the above discussion, we clarified that the excitation-energy dependences of the PL peaks of the thin film and the thick single crystal differ as a result of the different reabsorption effect. In the following, we discuss if there is a difference between the laser cooling efficiencies of the thick single crystal and the thin film. It is straightforward that a stronger PL at the high-energy side of the excitation energy would result in a higher cooling efficiency [25]. To proceed with the analysis, we define the S-PLE spectrum as the PLE spectrum obtained by the spectral integration of the low-energy side of the excitation energy, and the AS-PLE spectrum as that of the high-energy side.

In Fig. 2(a), we show the S-PLE and AS-PLE spectra for the thick single crystal as well as for the thin film. The PLE spectra are scaled by the excitation photon flux, and the PLE intensities are normalized by the totally integrated PL spectrum for the point E_{eq} where the S-PLE and AS-PLE

intensities are equal. Expressed in mathematical terms the intensities read

$$I_{\text{S-PLE}}(E_{ex}) = \frac{\int_0^{E_{ex}} I_{\text{PL}}(E, E_{ex}) dE}{\int_0^{\infty} I_{\text{PL}}(E, E_{eq}) dE}, \qquad (1)$$

$$I_{\text{AS-PLE}}(E_{ex}) = \frac{\int_{E_{ex}}^{\infty} I_{\text{PL}}(E, E_{ex}) dE}{\int_0^{\infty} I_{\text{PL}}(E, E_{eq}) dE}. \qquad (2)$$

Here, $I_{\text{PL}}(E, E_{ex})$ is the PL spectrum detected for the excitation energy E_{ex}. From the definition via the normalized spectra we have $I_{\text{S-PLE}}(E_{eq}) = I_{\text{AS-PLE}}(E_{eq}) = 0.5$. For excitation at this energy E_{ex}, it is considered that neither heating nor cooling of the system occurs if the external luminescence efficiency is unity. For the thin film, E_{eq} is 1.599 eV, and for the single crystal it is 1.530 eV. It can be considered that the E_{eq} of the thick single crystal is redshifted compared to the thin film, due to reabsorption.

First, we focus on the S-PLE spectra. In the energy range above the band edge, the shape of the S-PLE spectrum agrees with that of the common PLE spectrum monitored at the PL peak. Especially in the case of the thin film, this shape serves as an indicator of the absorption coefficient. Furthermore, due to the influence of the reabsorption effect in the thick single crystal, the excitation-energy dependence vanishes and a flat S-PLE structure is established [19]. For energies below the band edge, especially in the energy range below E_{eq}, the S-PLE intensity decays exponentially. Below we employ the fact
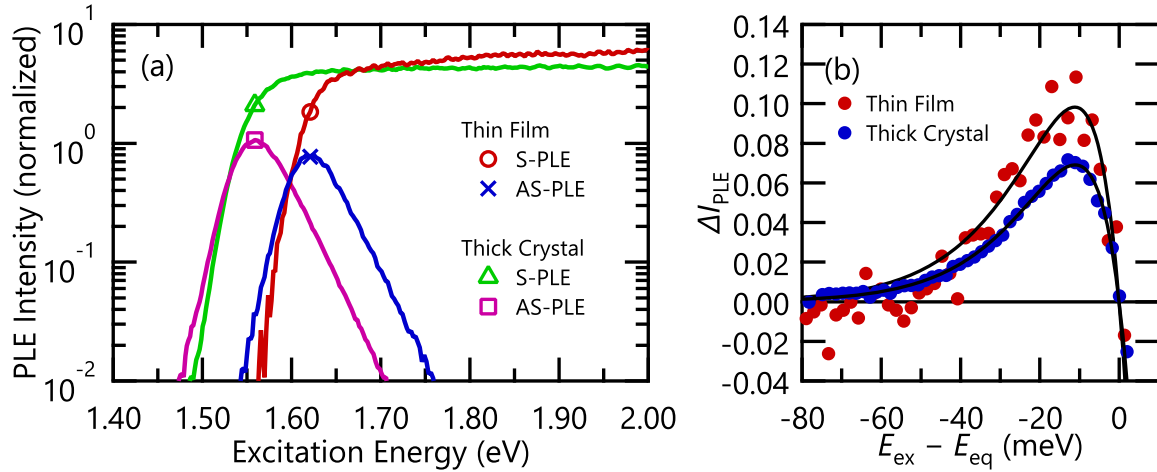
FIG. 2. (a) S-PLE (red) and AS-PLE (blue) spectra for the MAPbI$_3$ thin film, and S-PLE (green) and AS-PLE (pink) spectra for the MAPbI$_3$ thick single crystal. (b) The up-conversion gain spectrum (ΔI_{PLE}) of the MAPbI$_3$ thin film and thick single crystal plotted as a function of $E_{ex} - E_{eq}$ for easy comparison. The zero cross point of ΔI_{PLE} corresponds to $E_{ex} = E_{eq}$. The red and blue data stand for the thin film and thick single crystal, respectively. The solid lines are the fitting results using Eq. (5).

that this slope is related to the Urbach tail of the absorption spectrum.

Next, we focus on the AS-PLE spectra. The AS-PLE peak position was 1.620 eV for the thin film, and 1.559 eV for the single crystal. For an excitation energy corresponding to the AS-PLE peak position, the AS-PL intensity has its maximum (i.e., the AS-PL efficiency is maximized), but since this point is on the high-energy side of E_{eq}, it can be considered that no cooling of the semiconductor occurs. It is important to note that this peak energy position is determined by the absorption spectrum and the shape of the PL spectrum. Additionally, the peak position also redshifts through the influence of reabsorption in the single crystal.

We proceed by determining the excitation energy that maximizes the laser cooling efficiency and perform a comparison of the numerical values. It is expected that the laser cooling efficiency becomes maximum at the point where the difference between the AS-PLE and S-PLE intensities reaches its maximum. Therefore, we define that difference as the up-conversion gain spectrum. In Fig. 2(b), we show the experimentally obtained intensity difference ΔI_{PLE} ($\equiv I_{AS\text{-}PLE} - I_{S\text{-}PLE}$) for the thin film and the thick single crystal. It is clear that the signal-to-noise ratio of ΔI_{PLE} for the single crystal is much better than that for thin film. This is because the flat surface of the single crystal induces less scattering of excitation light [19]. We note that ΔI_{PLE} corresponds to the actual cooling rate when the external luminescence efficiency is unity. As a result, similar spectra were obtained for both the thin film and the thick single crystal. From Fig. 2(a), we find that in the region below E_{eq}, the $I_{S\text{-}PLE}$ and $I_{AS\text{-}PLE}$ exhibit a behavior that is similar to the exponential Urbach tail. Therefore, the following equations hold:

$$I_{S\text{-}PLE}(E_{ex}) = \tfrac{1}{2} e^{(E_{ex} - E_{eq})/E_S}, \tag{3}$$

$$I_{AS\text{-}PLE}(E_{ex}) = \tfrac{1}{2} e^{(E_{ex} - E_{eq})/E_{AS}}. \tag{4}$$

Here, we define E_S with the exponential slope of the S-PLE spectrum, and E_{AS} with that of the AS-PLE spectrum. Then, ΔI_{PLE} can be expressed as

$$\Delta I_{PLE}(E_{ex}) = \tfrac{1}{2} e^{(E_{ex} - E_{eq})/E_{AS}} - \tfrac{1}{2} e^{(E_{ex} - E_{eq})/E_S}. \tag{5}$$

We fitted the ΔI_{PLE} data using Eq. (5), and obtained the fitting results $E_S = 8.675$ meV and $E_{AS} = 14.90$ meV for the thin film, and $E_S = 9.253$ meV and $E_{AS} = 13.50$ meV for the single crystal. In addition, the Urbach energy E_U can be determined as follows (the derivation is given in Appendix C):

$$E_U = \frac{2 E_S E_{AS}}{E_S + E_{AS}}. \tag{6}$$

From Eq. (6), we obtained $E_U = 10.97$ meV for the thin film, and $E_U = 10.98$ meV for the single crystal. Since almost the same value was obtained, this value of the Urbach energy can be considered as an intrinsic parameter of MAPbI$_3$.

Moreover, the optimized excitation energy difference $E_{opt} - E_{eq}$, where ΔI_{PLE} is maximized, was -11.23 meV for the thin film and -11.11 meV for the single crystal. According to these values, we obtained that the energy difference $E_{opt} - E_{eq}$ is -11 meV for both thin and thick samples. This means that the cooling efficiency can be maximized for both samples when excitation light with an energy 11 meV below E_{eq} is employed. In addition, this value agrees well with E_U, and we can infer that the same mechanism, for example, carrier-phonon coupling, contributes to the Urbach tail of the absorption as well as to the PL up-conversion process in MAPbI$_3$. The broad shape of ΔI_{PLE} also resembles the broad energy distribution of phonons due to the vibrational and torsional modes of the organic cation MA [38] and suggests unique properties such as large anharmonic and overdamped phonons [39]. This is supported by the fact that the LO phonon mode derived from the halide cages of perovskites is strongly damped by the coupling between the MA cation modes and the LO phonon mode at room temperature [40].

C. Cooling efficiency

In the following, we evaluate the cooling efficiency reduction of the single crystal. The maximum values of ΔI_{PLE} were 0.09827 and 0.06908 for the thin film and single crystal, respectively. The single crystal's value is about 70% of that of the thin film, which is relatively small. This means that the cooling efficiency of the single crystal is actually reduced through the influence of the light confinement via photon reabsorption. On the other hand, it can be said that even for an extremely thick single crystal millimeters in size, the reduction is limited to 30% at most. According to a previous report, the cooling efficiency of a 3-μm-thick sample is only 43% of that of a 0.2-μm sample [29]. However, we have to bear in mind that the thick sample is influenced by photon reabsorption due to the increased sample thickness. It is obvious that the excitation energy for maximum cooling shifts as the film thickness increases due to the reabsorption effect. By utilizing our method, the optimized excitation energy can be determined for each sample.

Furthermore, the E_{eq} of the thick single crystal is redshifted through the reabsorption effect. However, independent of the sample thickness, the optimized excitation energy E_{opt} is 11 meV below E_{eq}. These facts suggest that by changing the film thickness the strength of the reabsorption can be altered and the required excitation energy for the optimum cooling efficiency can be controlled. In other words, the design of a device matched with the excitation laser energy becomes possible by controlling the film thickness. In addition, for a perovskite layer that is moderately thin, E_{eq} lies close to the PL peak energy. Therefore, the optimized excitation energy of a thin sample can be roughly estimated by measuring the PL peak energy.

So far, we discussed the cooling rate in case of an external luminescence efficiency that is unity. Below, we discuss the lower limit of the external luminescence efficiency for cooling. We define the cooling gain G_{c} with

$$G_{\text{c}} = \eta_{\text{ext}} \Delta I_{\text{PLE}} - (1 - \eta_{\text{ext}}). \tag{7}$$

Here, η_{ext} is the external luminescence efficiency. The first term expresses the cooling gain via luminescence, and the second represents the heating due to nonradiative losses. The system will be cooled when $G_{\text{c}} > 0$. The lower limit of η_{ext} for cooling can be calculated from the condition $G_c = 0$, resulting in 91.05% for the thin film and 93.53% for the thick crystal. Because of photon reabsorption, a more restrictive condition has to be fulfilled for the thick crystal. However, the detrimental effect of the film thickness is not severe in highly luminescent perovskites.

IV. CONCLUSION

In conclusion, we fabricated MAPbI₃ thin films and few-millimeter-thick single crystals. The AS-PL was clearly observed for both the thin film and the single crystal. Via PLE measurements we characterized their AS-PL features as well as their potential for laser cooling. We found that regardless of the sample, the cooling efficiency should be maximized when the excitation energy E_{ex} is about 11 meV below the energy E_{eq} which defines the balance between AS-PLE and S-PLE

intensities. For the single crystal, we estimated a cooling efficiency close to 70% of that for the thin film, indicating the possibility of laser cooling even in the thick single crystal.

APPENDIX A: ORIGIN OF THE REDSHIFTED SPECTRA OF SINGLE CRYSTALS

According to Fig. 1, we can confirm that the PL spectra from the thick single crystal were overall redshifted with respect to the thin film. This can be explained with the spatial distribution of photocarriers and the reabsorption effect [11,12,16,18–20]. When the excitation energy is above $\approx$1.6 eV, the PL peak energy is 1.552 eV and exhibits almost no further change. This peak position energy is small when compared with the peak position of the thin film (1.600 eV). For excitation energies that are sufficiently above the band gap, the absorption coefficient is large and thus the excited carriers are initially localized at the sample surface. In this case the difference between the carrier distributions of thin film and single crystal vanishes, and therefore the obtained PL spectra should become equal. However, in case of a long carrier diffusion length, the excited carrier distribution must expand into the sample's interior in proportion to this value. Consequently, the time-averaged carrier distribution will have a distribution that reaches deeper than the penetration depth of the excitation light, and through the PL reabsorption effect in the thick single crystal, a redshifted PL spectrum was observed when compared with the thin film. Additionally, the peak position 1.552 eV can be considered to reflect the carrier diffusion length in the single-crystal sample. When the excitation energy becomes lower than $\approx$1.6 eV, the PL peak redshifts accordingly. In this range the penetration depth of the excitation light becomes longer than the carrier diffusion length, and the carrier distribution expands deeper into the inside of the sample. Therefore, we can infer that the PL redshifted as a result of a stronger reabsorption effect.

APPENDIX B: DISCUSSION OF THE AS-PL RATIO

In Fig. 3 we plotted the excitation-energy dependence of the ratio between the intensities of the AS-PL and the total PL spectrum. Expressed in mathematical terms, this ratio is written as

$$R_{\text{AS}}(E_{\text{ex}}) = \frac{\int_{E_{\text{ex}}}^{\infty} I_{\text{PL}}(E, E_{\text{ex}}) \mathrm{d}E}{\int_{0}^{\infty} I_{\text{PL}}(E, E_{\text{ex}}) \mathrm{d}E}. \tag{B1}$$

When the spectral shape of I_{PL} is independent of E_{ex}, Eq. (B1) becomes simply the integration of the PL spectra, and the resulting shape is sigmoidlike. From the definition, we obtain $R_{\text{AS}}(E_{\text{eq}}) = 0.5$. The tail of R_{AS} at the high-energy side reflects the high-energy tail of I_{PL}. From the van Roosbroeck–Shockley relation [41], we understand that the numerical value of its slope corresponds to the thermal energy of the semiconductor. This energy was about 28 meV for both the
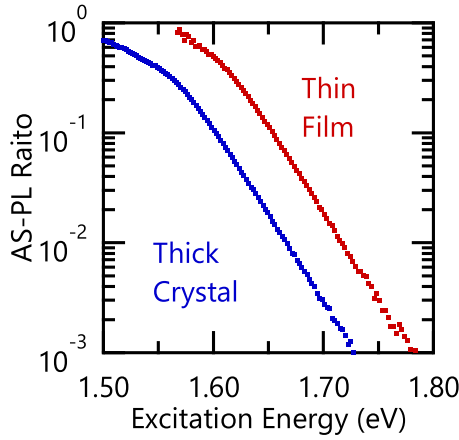
FIG. 3. Plot of the excitation-energy dependence of the ratio between the intensities of the AS-PL and the total PL spectrum. The red and blue dot lines are the dependence for the thin film and thick single crystal, respectively.

thin film and the thick single crystal. This is slightly larger than the room-temperature energy, which is attributed to the influence of the heating through the excitation light as S-PL dominates at the high-energy tail of R_{AS}. When we focus on the region close to E_{eq}, we find that, in the single crystal, the change of R_{AS} with respect to E_{ex} is gentler when compared with the thin film. Because in this range a shift of the PL peak also occurs due to the reabsorption, we consider that the inclination of R_{AS} became gentler.

APPENDIX C: DERIVATION OF THE URBACH ENERGY

To derive the value of the Urbach energy, we first discuss the meanings of E_S and E_{AS}. When we consider $I_{S\text{-PLE}}$ and $I_{AS\text{-PLE}}$ from the viewpoint of the general relation between the PLE spectra and absorption spectra, $I_{AS\text{-PLE}}$ should be proportional to the product of the absorption α_{ex} and the fraction of the AS-PL, R_{AS}. In the same manner, it can be suggested that $I_{S\text{-PLE}}$ is proportional to the product of α_{ex} and the fraction of the S-PL, $1-R_{AS}$. In other words, when we assign the Urbach energy of the absorption spectrum to

E_U and the slope of R_{AS} in the region below E_{eq} to E_U, the following equations hold:

$$I_{S\text{-PLE}}(E_{ex}) \propto \alpha_{ex}(1 - R_{AS}) \propto e^{(E_{ex}/E_U)+(E_{ex}/E_R)}, \qquad \text{(C1)}$$

$$I_{AS\text{-PLE}}(E_{ex}) \propto \alpha_{ex} R_{AS} \propto e^{(E_{ex}/E_U)-(E_{ex}/E_R)}. \qquad \text{(C2)}$$

Consequently, with respect to E_U and E_R the following two equations are satisfied:

$$E_U = \frac{2E_{AS}E_S}{E_{AS} + E_S}, \qquad \text{(C3)}$$

$$E_R = \frac{2E_{AS}E_S}{E_{AS} - E_S}. \qquad \text{(C4)}$$

When we determine E_U from Eq. (C3), we obtain 10.97 meV for the thin film, and 10.98 meV for the single crystal. Since almost the same value was obtained for the thin film and the single crystal, this value can be considered an intrinsic parameter of MAPbI$_3$. We also determined E_R from Eq. (C4), resulting in 41.54 meV for the thin film and 58.82 meV for the single crystal. These values match well with those estimated from the slopes of R_{AS} in Fig. 3. This confirms that the approximations in Eqs. (C1) and (C2) are sufficiently accurate.

APPENDIX D: CALCULATION OF THE UP-CONVERSION GAIN SPECTRUM

After we obtained the absorption spectrum of a certain sample, we can calculate the sample-thickness dependence of the up-conversion gain spectrum (which is essentially the intensity difference between AS-PLE and S-PLE intensities) under consideration of the photon recycling effect as outlined in the following:

(1) Calculation of the spontaneous emission spectrum

Using the van Roosbroeck–Shockley relation [41], the spontaneous emission spectrum can be calculated from the absorption spectrum.

(2) Calculation of the carrier depth profile

The steady-state solution of the carrier depth profile is derived from the one-dimensional diffusion rate equation.
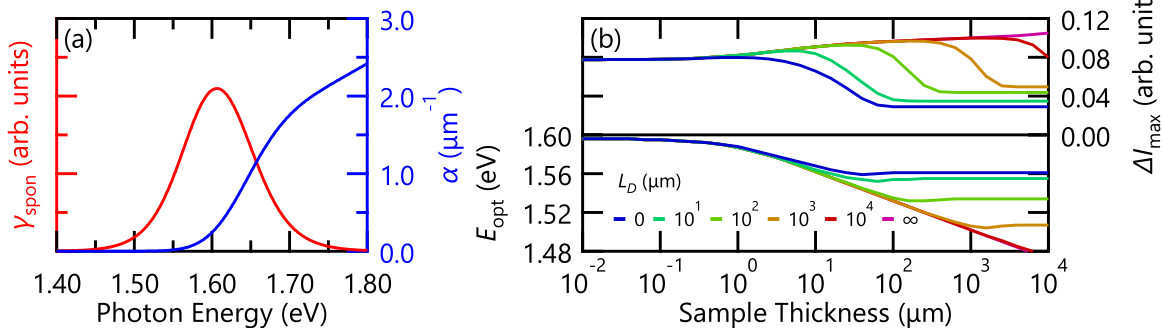
FIG. 4. (a) Spontaneous emission (red) and absorption (blue) spectra used for the calculation. These spectra are calculated from the ellipsometry data in Ref. [35]. (b) Theoretical sample-thickness dependence of the optimized excitation energy (E_{opt}, upper panel) and the maximum value of the up-conversion gain (ΔI_{max}, lower panel). L_D corresponds to the diffusion length of the sample including photon recycling effects.
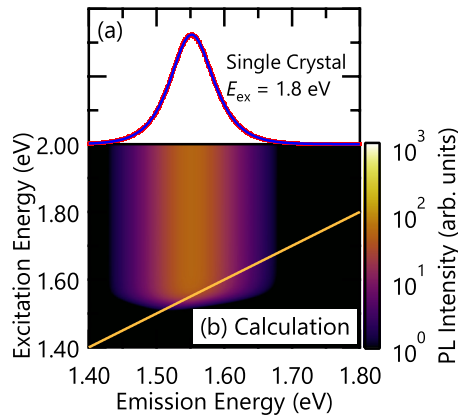
FIG. 5. (a) PL spectrum of the MAPbI$_3$ single crystal for an excitation energy of 1.8 eV. The red data shows to the experimental result and the blue line is the fitting result. (b) Calculated two-dimensional PLE map of the thick single crystal. The diagonal orange line is an eye guide indicating the excitation energy.

When we consider the terms for carrier generation, carrier diffusion, and carrier trapping, we can solve the equation analytically. The diffusion length here is not the one which can be directly derived from the carrier mobility of the material, because in this case the effect of photon recycling on this value has to be involved.

(3) Calculation of the PL spectrum

Here, we assume that the PL emission is dominated by bimolecular recombination and that the observed PL spectrum can be explained by combining the carrier depth profile and the reabsorption effect:

$$I_{\text{PL}}(E) \propto \gamma_{\text{spon}}(E) \int_0^L n(z)^2 e^{-\alpha z} \mathrm{d}z. \qquad \text{(D1)}$$

Here, $\gamma_{\text{spon}}(E)$, L, $n(z)$, and $\alpha(E)$ are the spontaneous emission spectrum, the sample thickness, the carrier depth profile,

and the absorption spectrum, respectively. By changing the excitation energy, we can obtain the two-dimensional PLE map.

(4) Calculation of ΔI_{PLE} from the obtained PLE map

We divide the calculated PLE data into Stokes and anti-Stokes parts and calculate the up-conversion gain spectrum. Then, we can determine the optimized excitation energy E_{opt} and the maximum value of the up-conversion gain ΔI_{max}.

(5) Performing the above steps with different thickness

For the calculation, we use the ellipsometry data in Ref. [35]. The calculated spontaneous emission and absorption spectra are shown in Fig. 4(a). The emission spectrum is almost the same as the PL spectrum obtained from the thin-film sample. Figure 4(b) provides the sample-thickness dependences of E_{opt} and ΔI_{max} in the upper and lower panels, respectively. According to Fig. 4(b), ΔI_{max} can be enhanced by increasing the sample thickness if the diffusion length (L_D) is sufficiently long. This is due to the volume effect of the sample. It is also clear that E_{opt} redshifts as the thickness increases.

APPENDIX E: CALCULATION OF THE REDSHIFTED SPECTRA OF SINGLE CRYSTALS

We can also perform the fitting of the redshifted PL spectrum data obtained from the single crystals by employing the procedures (1) to (3) as outlined in the previous section. In Fig. 5(a), we show the experimental data and the fitting result for an excitation energy of 1.8 eV. For the fitting, we used the absorption and spontaneous emission spectra in Fig. 4(a), and a sample thickness of 1.5 mm. The diffusion length L_D is used as a free-fitting parameter and we obtained $L_D = 178\,\mu\text{m}$, which is consistent with the previous report [10]. The calculated two-dimensional PLE map shown in Fig. 5(b) matches the experimentally obtained map shown in Fig. 1(b) very well. This shows that the redshifted spectra of single crystals are a result of the carrier diffusion and reabsorption effect.

[1] A. Kojima, K. Teshima, Y. Shirai, and T. Miyasaka, Organometal halide perovskites as visible-light sensitizers for photovoltaic cells, J. Am. Chem. Soc. **131**, 6050 (2009).

[2] M. M. Lee, J. Teuscher, T. Miyasaka, T. N. Murakami, and H. J. Snaith, Efficient hybrid solar cells based on meso-superstructured organometal halide perovskites, Science **338**, 643 (2012).

[3] H.-S. Kim, C.-R. Lee, J.-H. Im, K.-B. Lee, T. Moehl, A. Marchioro, S.-J. Moon, R. Humphry-Baker, J.-H. Yum, J. E. Moser, M. Grätzel, and N.-G. Park, Lead iodide perovskite sensitized all-solid-state submicron thin film mesoscopic solar cell with efficiency exceeding 9%, Sci. Rep. **2**, 591 (2012).

[4] NREL, Research Cell Record Efficiency Chart, https://www.nrel.gov/pv/assets/pdfs/pv-efficiency-chart.20190103.pdf

[5] S. D. Stranks, G. E. Eperon, G. Grancini, C. Menelaou, M. J. P. Alcocer, T. Leijtens, L. M. Herz, A. Petrozza, and H. J. Snaith, Electron-hole diffusion lengths exceeding 1 micrometer in an organometal trihalide perovskite absorber, Science **342**, 341 (2013).

[6] G. Xing, N. Mathews, S. Sun, S. S. Lim, Y. M. Lam, M. Grätzel, S. Mhaisalkar, and T. C. Sum, Long-range balanced electron-and hole-transport lengths in organic-inorganic CH₃NH₃PbI₃, Science **342**, 344 (2013).

[7] Y. Yamada, T. Nakamura, M. Endo, A. Wakamiya, and Y. Kanemitsu, Near-band-edge optical responses of solution-processed organic–inorganic hybrid perovskite CH₃NH₃PbI₃ on mesoporous TiO₂ electrodes, Appl. Phys. Exp. **7**, 032302 (2014).

[8] S. D. Wolf, J. Holovsky, S.-J. Moon, P. Löper, B. Niesen, M. Ledinsky, F.-J. Haug, J.-H. Yum, and C. Ballif, Organometallic halide perovskites: Sharp optical absorption edge and its relation to photovoltaic performance, J. Phys. Chem. Lett. **5**, 1035 (2014).

[9] Y. Yamada, T. Nakamura, M. Endo, A. Wakamiya, and Y. Kanemitsu, Photocarrier recombination dynamics in perovskite CH₃NH₃PbI₃ for solar cell applications, J. Am. Chem. Soc. **136**, 11610 (2014).

[10] Q. Dong, Y. Fang, Y. Shao, P. Mulligan, J. Qiu, L. Cao, and J. Huang, Electron-hole diffusion lengths >175 μm in solution-grown $CH_3NH_3PbI_3$ single crystals, Science **347**, 967 (2015).

[11] Y. Yamada, T. Yamada, L. Q. Phuong, N. Maruyama, H. Nishimura, A. Wakamiya, Y. Murata, and Y. Kanemitsu, Dynamic optical properties of $CH_3NH_3PbI_3$ single crystals as revealed by one- and two-photon excited photoluminescence measurements, J. Am. Chem. Soc. **137**, 10456 (2015).

[12] T. Yamada, Y. Yamada, H. Nishimura, Y. Nakaike, A. Wakamiya, Y. Murata, and Y. Kanemitsu, Fast free-carrier diffusion in $CH_3NH_3PbBr_3$ single crystals revealed by time-resolved one- and two-photon excitation photoluminescence spectroscopy, Adv. Electron. Mater. **2**, 1500290 (2016).

[13] L. M. Pazos-Outón, M. Szumilo, R. Lamboll, J. M. Richter, M. Crespo-Quesada, M. Abdi-Jalebi, H. J. Beeson, M. Vrućinić, M. Alsari, H. J. Snaith, B. Ehrler, R. H. Friend, and F. Deschler, Photon recycling in lead iodide perovskite solar cells, Science **351**, 1430 (2016).

[14] J. M. Richter, M. Abdi-Jalebi, A. Sadhanala, M. Tabachnyk, J. P. H. Rivett, L. M. Pazos-Outón, K. C. Gödel, M. Price, F. Deschler, and R. H. Friend, Enhancing photoluminescence yields in lead halide perovskites by photon recycling and light out-coupling, Nat. Commun. **7**, 13941 (2016).

[15] Y. Fang, H. Wei, Q. Dong, and J. Huang, Quantification of re-absorption and re-emission processes to determine photon recycling efficiency in perovskite single crystals, Nat. Commun. **8**, 14417 (2017).

[16] T. Yamada, Y. Yamada, Y. Nakaike, A. Wakamiya, and Y. Kanemitsu, Photon emission and reabsorption processes in $CH_3NH_3PbBr_3$ single crystals revealed by time-resolved two-photon-excitation photoluminescence microscopy, Phys. Rev. Appl. **7**, 014001 (2017).

[17] F. Staub, T. Kirchartz, K. Bittkau, and U. Rau, Manipulating the net radiative recombination rate in lead halide perovskite films by modification of light outcoupling, J. Phys. Chem. Lett. **8**, 5084 (2017).

[18] Y. Yamada, M. Hoyano, R. Akashi, K. Oto, and Y. Kanemitsu, Impact of chemical doping on optical responses in bismuth-doped $CH_3NH_3PbBr_3$ single crystals: Carrier lifetime and photon recycling, J. Phys. Chem. Lett. **8**, 5798 (2017).

[19] T. Yamada, T. Aharen, and Y. Kanemitsu, Near-Band-Edge Optical Responses of $CH_3NH_3PbCl_3$ Single Crystals: Photon Recycling of Excitonic Luminescence, Phys. Rev. Lett. **120**, 057404 (2018).

[20] Y. Yamada, T. Yamada, and Y. Kanemitsu, Free carrier radiative recombination and photon recycling in lead halide perovskite solar cell materials, Bull. Chem. Soc. Jpn. **90**, 1129 (2017).

[21] M. Sheik-Bahae and R. I. Epstein, Optical refrigeration, Nat. Photonics **1**, 693 (2007).

[22] R. I. Epstein, M. I. Buchwald, B. C. Edwards, T. R. Gosnell, and C. E. Mungan, Observation of laser-induced fluorescent cooling of a solid, Nature (London) **377**, 500 (1995).

[23] D. V. Seletskiy, S. D. Melgaard, S. Bigotta, A. D. Lieto, M. Tonelli, and M. Sheik-Bahae, Laser cooling of solids to cryogenic temperatures, Nat. Photonics **4**, 161 (2010).

[24] S. D. Melgaard, A. R. Albrecht, M. P. Hehlen, and M. Sheik-Bahae, Solid-state optical refrigeration to sub-100 Kelvin regime, Sci. Rep. **6**, 20380 (2016).

[25] M. Sheik-Bahae and R. I. Epstein, Can Laser Light Cool Semiconductors?, Phys. Rev. Lett. **92**, 247403 (2004).

[26] H. Gauck, T. H. Gfroerer, M. J. Renn, E. A. Cornell, and K. A. Bertness, External radiative quantum efficiency of 96% from a GaAs/GaInP heterostructure, Appl. Phys. A **64**, 143 (1997).

[27] E. Finkeißen, M. Potemski, P. Wyder, L. Viña, and G. Weimann, Cooling of a semiconductor by luminescence up-conversion, Appl. Phys. Lett. **75**, 1258 (1999).

[28] D. A. Bender, J. G. Cederberg, C. Wang, and M. Seik-Bahae, Development of high quantum efficiency GaAs/GaInP double heterostructures for laser cooling, Appl. Phys. Lett. **102**, 252102 (2013).

[29] S.-T. Ha, C. Shen, J. Zhang, and Q. Xiong, Laser cooling of organic–inorganic lead halide perovskites, Nat. Photonics **10**, 115 (2016).

[30] Y. Kanemitsu and T. Handa, Photophysics of metal halide perovskites: From materials to devices, Jpn. J. Appl. Phys. **57**, 090101 (2018).

[31] K. Kojima, T. Ohtomo, K. Ikemura, Y. Yamazaki, M. Saito, H. Ikeda, K. Fujito, and S. F. Chichibu, Determination of absolute value of luminescence efficiency of radiation in high quality GaN single crystals using an integrating sphere, J. Appl. Phys. **120**, 015704 (2016).

[32] N. J. Jeon, J. H. Noh, Y. C. Kim, W. S. Yang, S. Ryu, and S. I. Seok, Solvent engineering for high-performance inorganic–organic hybrid perovskite solar cells, Nat. Mater. **13**, 897 (2014).

[33] M. I. Saidaminov, A. L. Abdelhady, G. Maculan, and O. M. Bakr, Retrograde solubility of formamidinium and methylammonium lead halide perovskites enabling rapid single crystal growth, Chem. Commun. **51**, 17658 (2015).

[34] C. Wehrenfennig, M. Liu, H. J. Snaith, M. B. Johnston, and L. M. Herz, Homogeneous emission line broadening in the organo lead halide perovskite $CH_3NH_3PbI_{3-x}Cl_x$, J. Phys. Chem. Lett. **5**, 1300 (2014).

[35] M. Shirayama, H. Kadowaki, T. Miyadera, T. Sugita, M. Tamakoshi, M. Kato, T. Fujiseki, D. Murata, S. Hara, T. N. Murakami, S. Fujimoto, M. Chikamatsu, and H. Fujiwara, Optical Transitions in Hybrid Perovskite Solar Cells: Ellipsometry, Density Functional Theory, and Quantum Efficiency Analyses for $CH_3NH_3PbI_3$, Phys. Rev. Appl. **5**, 014012 (2016).

[36] K. Galkowski, A. Mitioglu, A. Miyata, P. Plochocka, O. Portugall, G. E. Eperon, J. T.-W. Wang, T. Stergiopoulos, S. D. Stranks, H. J. Snaith, and R. J. Nicholas, Determination of the exciton binding energy and effective masses for methylammonium and formamidinium lead tri-halide perovskite semiconductors, Energy Environ. Sci. **9**, 962 (2016).

[37] F. Urbach, The long-wavelength edge of photographic sensitivity and electronic absorption of solids, Phys. Rev. **92**, 1324 (1953).

[38] C. Quarti, G. Grancini, E. Mosconi, P. Bruno, J. M. Ball, M. M. Lee, H. J. Snaith, A. Petrozza, and F. D. Angelis, The Raman spectrum of the $CH_3NH_3PbI_3$ hybrid perovskite: Interplay of theory and experiment, J. Phys. Chem. Lett. **5**, 279 (2014).

[39] M. Sendner, P. K. Nayak, D. A. Egger, S. Beck, C. Müller, B. Epding, W. Kowalsky, L. Kronik, H. J. Snaith, A. Pucci, and R. Lovrinčić, Optical phonons in methylammonium lead halide

perovskites and implications for charge transport, Mater. Horiz. **3**, 613 (2016).

[40] M. Nagai, T. Tomioka, M. Ashida, M. Hoyano, R. Akashi, Y. Yamada, T. Aharen, and Y. Kanemitsu, Longitudinal Optical Phonons Modified by Organic Molecular Cation Motions in Organic-Inorganic Hybrid Perovskites, Phys. Rev. Lett. **121**, 145506 (2018).

[41] W. van Roosbroeck and W. Shockley, Photon-radiative recombination of electrons and holes in germanium, Phys. Rev. **94**, 1558 (1954).